Final Technical Report

Project Title:
Robust Estimation of Fault Slip, Block Rotation and Off-Fault Strain Rates in the Walker Lane from GPS Data

USGS NEHRP Award number: G17AP00004

Principal Investigator:
William C. Hammond, whammond@unr.edu

Contact Information:
Nevada Bureau of Mines and Geology
University of Nevada, Reno
1664 N. Virginia Street, Reno, NV 89557
Tel: 775-784-6436; Fax: 775-784-1709

Start and End Dates of this 12 Month Project:
December 1, 2016 to November 30, 2017

Abstract

In this project a new method is developed and used to combine, filterer and interpolate horizontal GPS velocity data in California and Nevada to image strain rates and fault slip rates in Walker Lane Belt (WLB) in the western Great Basin. I use GPS Imaging to combine GPS velocity fields, perform median-based despeckling and robust interpolation to obtain a gridded velocity field, and derive from it a strain rate field. The strain rate model shows, in addition to the well-known active tectonic transtension in the WLB east of the Sierra Nevada/Great Valley microplate, clearly delineated domains affected by anomalies associated with transient magmatic inflation at LVC, contraction near Lassen Peak, and positive dilatation associated transient earthquake cycle-related deformation at the Central Nevada Seismic Belt.

To obtain slip rates on faults in the WLB from the velocity field I have developed a new method, called Spontaneous Blocks, where the block model generates itself automatically around a given fault database. Automatic generation of block boundaries is advantageous because it provides for multiple estimates of slip rate on every fault in different realization of the block construction, thus providing a means to estimate realistic uncertainties attributable to block representation, and allows for more comprehensive exploration of the effects of different regularizations and fault databases on the set of derived slip rates. This is especially useful in areas like the WLB were there are many faults, forming complex networks, variable strain rates, and building of individual block models is labor intensive.

Introduction

The Walker Lane Belt (WLB) in the western part of the Intermountain West region of the western United States faces the threat of future earthquakes that can damage property, cause loss of life, and disrupt infrastructure and economic activity. Every year approximately 20-25% of the tectonic relative motion between the Pacific and North American plates gets accommodated east of the Sierra Nevada, mostly in the WLB, driving the regional seismic hazard. The USGS recognizes this hazard and is tasked with developing the National Probabilistic Seismic Hazard Maps (PSHM), the latest edition of which is documented in *Petersen et al.,* (2014a). These maps continue to improve as the underlying datasets and methodologies are further developed (*Anderson and Biasi*, 2016). A fundamental input into the PSHM is the rate at which seismic moment is released in earthquakes, usually parameterized as a slip rate on known faults. Thus it is very important to obtain accurate and well-justified slip rates estimates on active faults. There are several challenges in doing this in the WLB, but an important observation for seismic hazard assessment is that the slip rates estimated in geologic studies, smoothed seismicity, and the geodetic strain rates are highly correlated (e.g., *Ward*, 1998; *Pancha et al.,* 2006; *Petersen et al.*, 2014a; *Bird and Kreemer,* 2014). This observation highlights the reciprocity between data collected during different stages of the seismic cycle, and the power of using a combination of all three datasets to assess seismic hazard. Each data type has its own strengths, limitations, and level of maturity in the methodologies used to ingest the data to the PSHM. Here we explore the extent to which GPS geodesy can independently constrain slip rates given geometric data on the trace of faults.

In the Walker Lane, making estimates of fault slip rates can be particularly challenging for several reasons. Many of the active faults have long recurrence times and hence there are few events in historic or recent geologic time to study in detailed geologic investigations (e.g., *Ramelli et al.,* 1999; *Caskey et al.,* 2004; *Bell et al.,* 2004*; Lee et al*., 2001; *Briggs and Wesnousky*, 2004; *Wesnousky*, 2005; *Koehler and Wesnousky*, 2011; *Amos et al*., 2015; *Haddon et al.*, 2016 to name a very few). Furthermore, the deformation field is complex and transtensional with hundreds of dextral, normal, and sinistral faults, folds, anticlines, and oroclinal flexures that accommodate relative motion (e.g., *Stewart*, 1988; *Oldow et al.,* 2001; *Oldow*, 2003; *Wesnousky*, 2005; *Faulds and Henry*, 2008, again naming only a very few). Styles of slip can vary within a single basin, faults often terminate without continuation into to other fault systems, which can make representation with simple block models challenging. Not all deformation occurs on large, range-bounding, or basin-dividing, through-going fault structures (*Wesnousky et al*, 2012). Thus a significant fraction of the deformation budget may be "off-fault" in the sense that the measured strain accumulation consistent with tectonic boundary conditions is not released in earthquakes on the narrow fault traces.

GPS networks help address some of these issues by placing strong constraints on budgets of deformation across fault zones over extended areas, that has occurred in the decades up to the present time. These data are complementary in space and time to geologic studies that map, date, and quantify past strain release at specific active fault zones. Integrating these measurements is a modeling task that uses the short term geodetic measurements to infer long term relative rate of motion of adjacent crustal blocks separated by the fault (e.g. *Savage and Burford*, 1973; *Bennett et al.,* 1999; *McCaffrey*, 2002; *Meade and Hagar*, 2005). While geodetic coverage across the western United States has expanded dramatically over the last two decades (Figure 1), and knowledge of the location and slip history of active faults have greatly improved (see e.g. the databases like the USGS Quaternary Fault and Fold Database - USGS QFFD), pulling these datasets together into a kinematically self-consistent framework that honors all data and physical principals has been challenging (*Petersen et al.*, 2014b). On the scale of the WLB modeling faults and block rotations on a system scale is possible, but involves labor intensive block construction whose uncertainties are difficult to assess (*Hearn and Humphreys*, 1998; *Hammond et al.*, 2011; *Bormann et al.*, 2013).

To summarize, challenges in estimating slip rates on a system scale throughout the WLB with GPS geodesy include 1) incomplete fault data, 2) incomplete GPS data, 3) limitations in model representations of fault networks, 4) the potential presences of off-fault/aseismic strain, and 5) the presence of earthquake cycle effects in geodetic data. In this project I focus on 2) and 3) above by using GPS Imaging to integrate all available GPS data, applying robust estimation techniques to filter and interpolate the velocity field. Then I perform the slip rate analysis using a new class of block modeling called “Spontaneous Blocks” that combines the strengths of classic elastic block models and crustal strain rate maps. If block models and continuum strain rate models (e.g. *Kreemer et al.*, 2012; 2014) represent end-members of modeling style, the technique used here lies between the end-members, closer to the block modeling strategy at some points and closer to the strain maps at other points in the analysis. The solution incorporates principals of robust estimation into the slip rate calculations, incorporating medians rather than means at key points, reducing the impact of data outliers on the input velocity field, fault complexity, and analyst choice in the development of block models. The method is a new variant on GPS Imaging (*Blewitt et al*., 2016; *Hammond et al., 2016*) which has been developed to make other aspects of GPS data interpretation more objective, repeatable, less sensitive to outliers and to provide defensible uncertainties.

Analysis

The method proposed here extends the regularized many-block method. The method will systematically and objectively generate block models from the input fault geometries and use an interpolated GPS velocity field to provide stability and robustness in slip rate estimation. The method will result in slip rates that account for adjacent block rotations and also partition the strain rates into those, and those not, attributable to known faults. Because blocks are generated automatically and the deformation solution regularized, having large numbers of blocks is not a problem. This will reduce the time and effort needed to generate models, allowing more

hypothesis testing of other parameters. It will also eliminate the need to have large overly-simplified blocks that resulted in unrealistically large slip rates on a few faults near the edges of large blocks (e.g. the Hammond/Bormann models in *Petersen et al.,* 2014b).

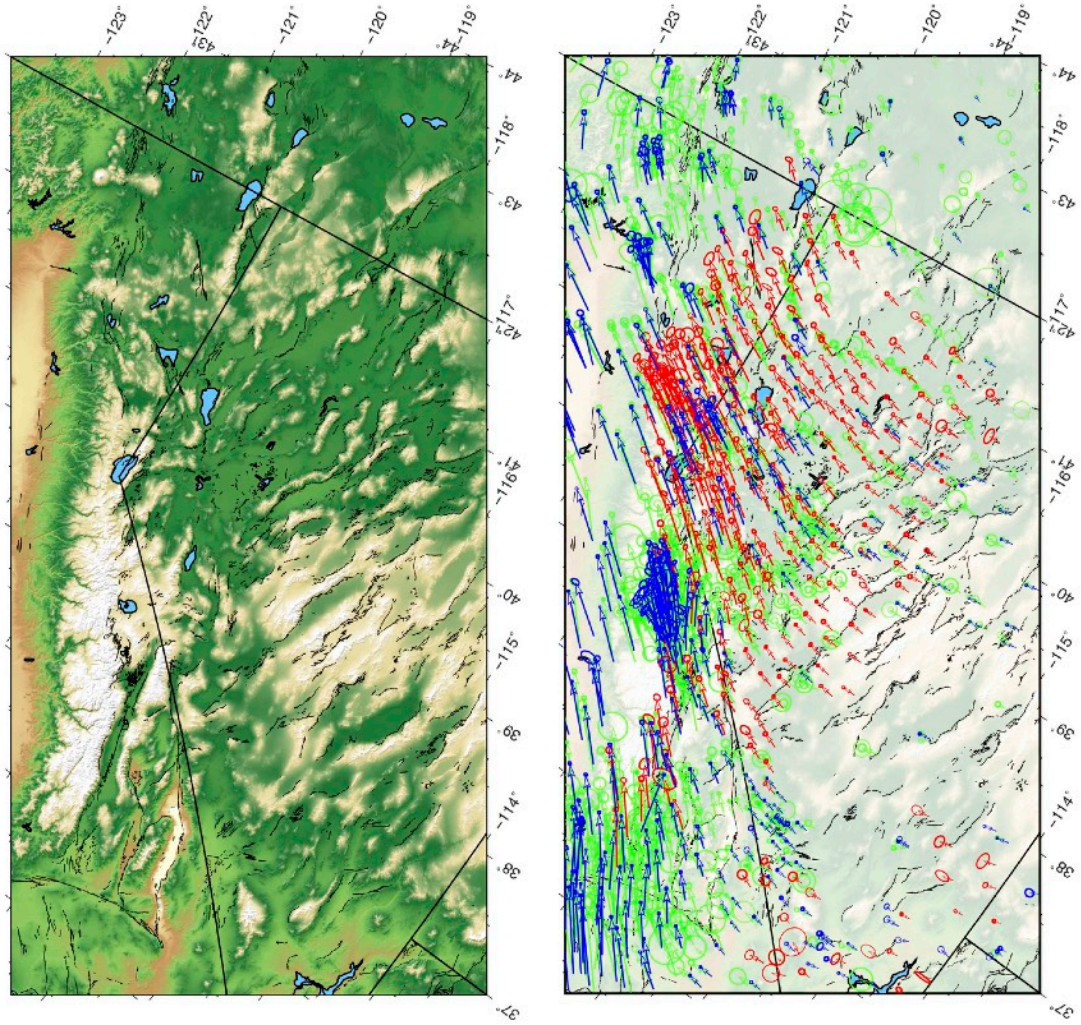

Figure 1. Topography and faults in the Walker Lane (left) and GPS velocities from the MAGNET GPS Network (red), Continuous GPS networks (blue), and USGS Campaign GPS networks (green). Velocity uncertainty ellipses are 95% confidence.

Velocity Field

To maximize geodetic coverage we integrate GPS data from our own MAGNET semi-continuous network that covers the entire WLB, with velocity fields from the USGS campaign GPS networks and the regional continuous GPS networks, such as the NSF EarthScope Plate Boundary Observatory. At the Nevada Geodetic Laboratory (NGL) we process all the original RINEX data from MAGNET plus all data from openly available continuous stations. After

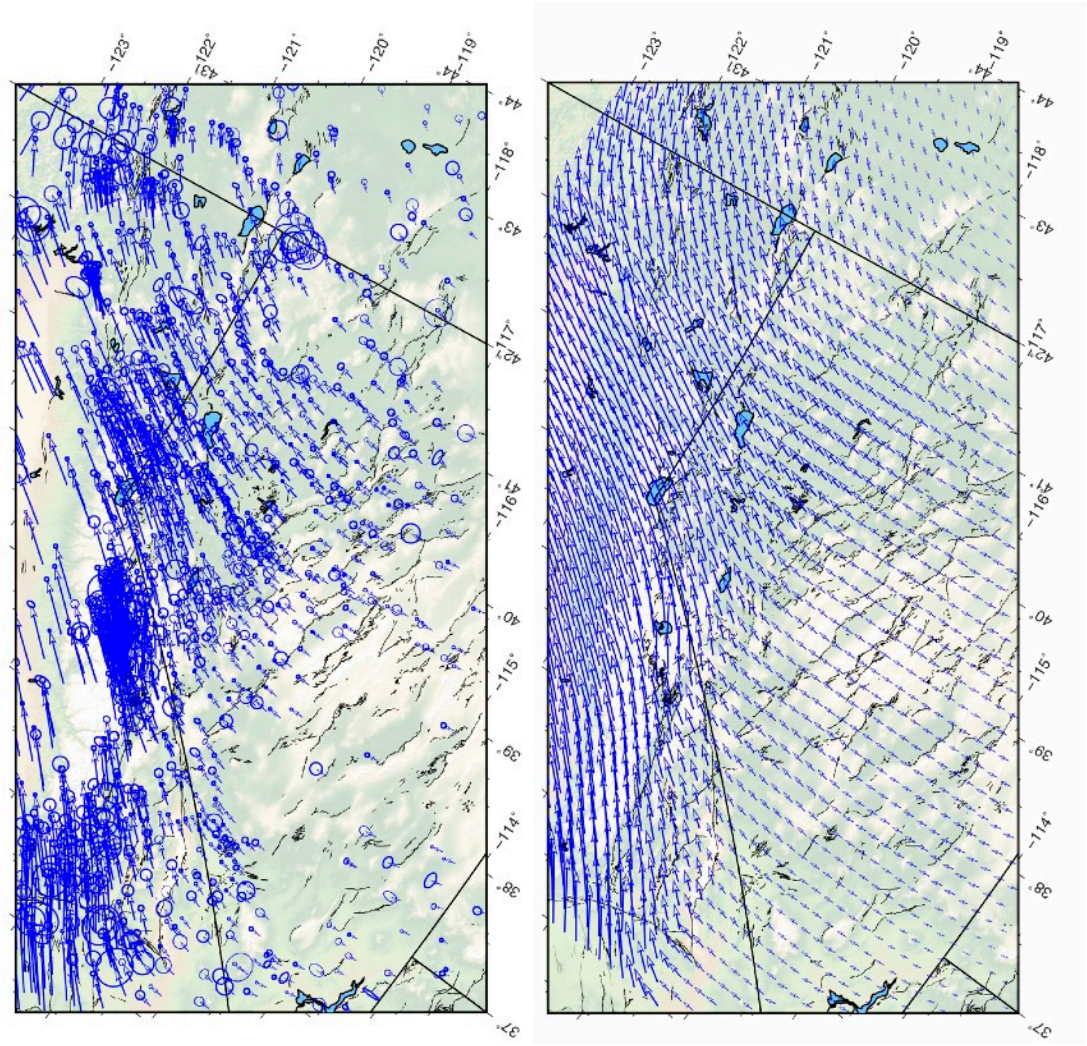

Figure 2. Integrated, aligned and declustered velocity field in NA12 reference frame (left). Gridded velocity field obtained using the GPS Imaging algorithm.

processing the data with the GIPSY software (detailed methodology provided at http://geodesy.unr.edu/gps/ngl.acn.txt), we use the MIDAS algorithm (*Blewitt et al.*, 2016) to estimate a trend from the position time series. MIDAS is a robust trend estimator that is highly insensitive to undocumented steps, outliers, seasonality, and heteroscedasticity, and provides realistic uncertainties that accounts for time series scatter and non-linearity. The method is non-parametric and based on Theil-Sen statistics and so does not rely on a specific model for the noise, e.g. power law (*Williams,* 2003). The rate estimate is the median of the distribution of rates based on pairs of data separated by approximately one year. Since it is based on medians, the result is insensitive to the tails of the distribution (occupied by outlying positions and steps). The method is computationally efficient and is useful for deriving a velocity field from large datasets such as those now available from the major processing groups. For the analysis presented here we use MIDAS on all continuous and MAGNET semi-continuous stations within the geographic area of interest and that have time series over 3.5 years in duration. We update the MIDAS rates for all stations processed at NGL weekly and place the files in NA12 and

IGS08 frames on our website (e.g., http://geodesy.unr.edu/velocities/midas.NA12.txt). The velocities in a North America reference frame (NA12, *Blewitt et al,* 2013) for the WLB are shown in Figure 1.

In the next stage we align other velocity fields that are available in various published forms to the MIDAS-generated field. This begins with selecting 10 of the USGS campaign GPS velocity fields that overlap with our area. These were obtained from https://earthquake.usgs.gov/monitoring/gps. The network names are given in Table 1.

Table 1. USGS Campaign GPS Network Names combined with the MIDAS NA12 GPS velocity field
BasinAndRange_SGPS
EasternORWA_SGPS
Mammoth_SGPS
NCalifornia_SGPS
ECSZ_SGPS
NorthEasternCal_SGPS
Sisters
BasinAndRange
LongValley
NCalifornia
The link to the file containing velocity data is: https://earthquake.usgs.gov/monitoring/gps/data/networks/<netname>/nafixed_velocity_file

In most cases the USGS processes data from some of the same regional continuous GPS or MAGNET semi-continuous stations that are processed by NGL, so that stations common between the velocity fields can be identified and used to estimate a rotation that minimizes the misfit between the two velocity fields. However, having stations in common between the two fields is not absolutely required because I use GPS Imaging to perform robust interpolation of one velocity field onto the stations of the other. This ensures that the fields fit together in their zone of overlap and that the rotation is insensitive to noise in the common stations. After the USGS networks are included I add the compilation of Kreemer et al., 2012 using the same process, which adds velocities in tables of other published studies. Following the alignments I decluster the combined GPS velocity field to combine multiple records for stations with 0.5 km of one another into a single record with a median rate for the group.

In the block modeling described below a gridded velocity field will be used so that every block will be covered by multiple estimates of the GPS velocity field, and areas with dense GPS coverage will not overwhelm areas with sparse coverage in the inversion for block rotations and slip rates. I grid the velocity field using the median spatial filter and GPS Imaging robust interpolator described in *Hammond et al.,* (2016). The algorithm was originally applied to vertical data, but here it is applied individually to the east and west velocity components, interpolating onto a 0.05 degree regular grid (Figure 2). At every point in the field GPS Imaging estimates the rate at the evaluation point based only on stations connected to it via a Delaunay triangulation. Thus, while the resulting signal is based on multiple stations and removes noise, it does not smooth the velocity field in the classic sense. The method will preserve step discontinuities in the velocity field (e.g. at a creeping fault) to the extent that the GPS network is dense enough to resolve it. Thus the resulting velocity field shown in Figure 2 is filtered but not smoothed except on the scale between adjacent stations. Thus its apparent smoothness is a real feature of the dataset and not an artifact of the analysis.

The resulting field shows the counter clockwise rotation of the Sierra Nevada/Great Valley microplate, and opposite sense of rotation of the northernmost WLB/Southern Oregon Basin and Range. The change in sign of rotation falls within the WLB at all latitudes of the system, suggesting that these two domains respond to different combinations of the tectonic forces.

Strain Rate Field

Once the GPS velocities have undergone robust interpolation onto a regular grid estimating the strain rate field is stabilized. Since the field is now filtered and free of outliers the velocity gradients have less noise and strain rates can be estimated with least squares. To get the fields shown in Figure 3abc the strain rates are estimated on a sphere using the relations of *Savage et al.*, (2001), with a moving window and Gaussian distance weighting function similar to the method of *Shen et al.,* (1996), using a half-width of 12 km. The colors in Figure 3a show the $\log_{10}$ of the magnitude of tensor strain rate, with magnitude defined as $e_{mag} = (e_{xx}^2 + e_{yy}^2 + 2e_{xy}^2)^{1/2}$ where e_{xx} e_{yy} and e_{xy} are the tensor strain rate components (*Kreemer et al.*, 2014). Figure 3b shows the shear component of tensor strain rate, where shear is defined as e_1-e_2 where e_1 and e_2 are the principal strain rate components. Figure 3c shows the dilatational component of strain rate defined as e_1+e_2.

The map shows high strain rates along the San Andreas fault system to the west, the medium-high strain rates in the WLB (generally less than 100 nanostrain/year). In the WLB the strain rates are highest where the contours of velocity are the most dense in the southern Walker Lane, near the Owens Valley and Sierra Nevada Range front, similar in location to a sharp gradient in vertical GPS velocity imaged in *Hammond et al.,* (2016).

Figure 3 also shows some poorly understood variations of the very low strain rates east of the Walker Lane in the eastern Nevada Basin and Range. These strain rates are generally lower than 5 nanostrain/yr and are near the uncertainties, thus it is not clear that they are significant. Some

of these anomalies may represent real variations in the crustal strain rates across the Basin and Range, while others may be artifacts of the GPS Imaging technique which tends to partition the velocity field into domains when the GPS station spacing is sparse, such as is the case north of Highway 80 and south of Highway 50 in Nevada.

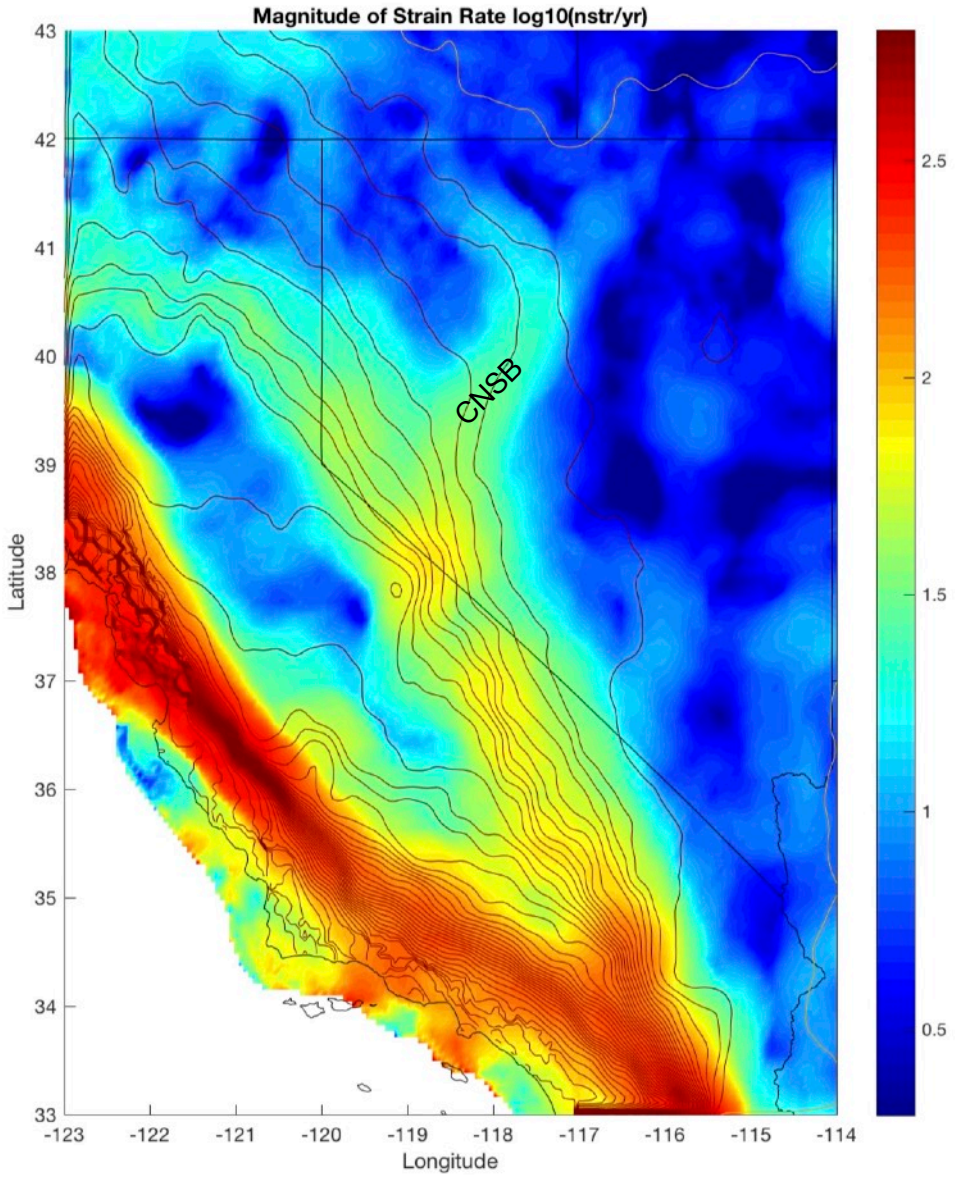

Figure 3a. Magnitude of tensor strain rate, cool colors are low strain rates, hot colors high strain rates. Color scale indicates strain rate in log10(nanostrain/year), black velocity contours are in intervals of 1 mm/yr. "CNSB" shows the location of the strain rate anomaly associated with viscoelastic relaxation following the Central Nevada earthquakes.

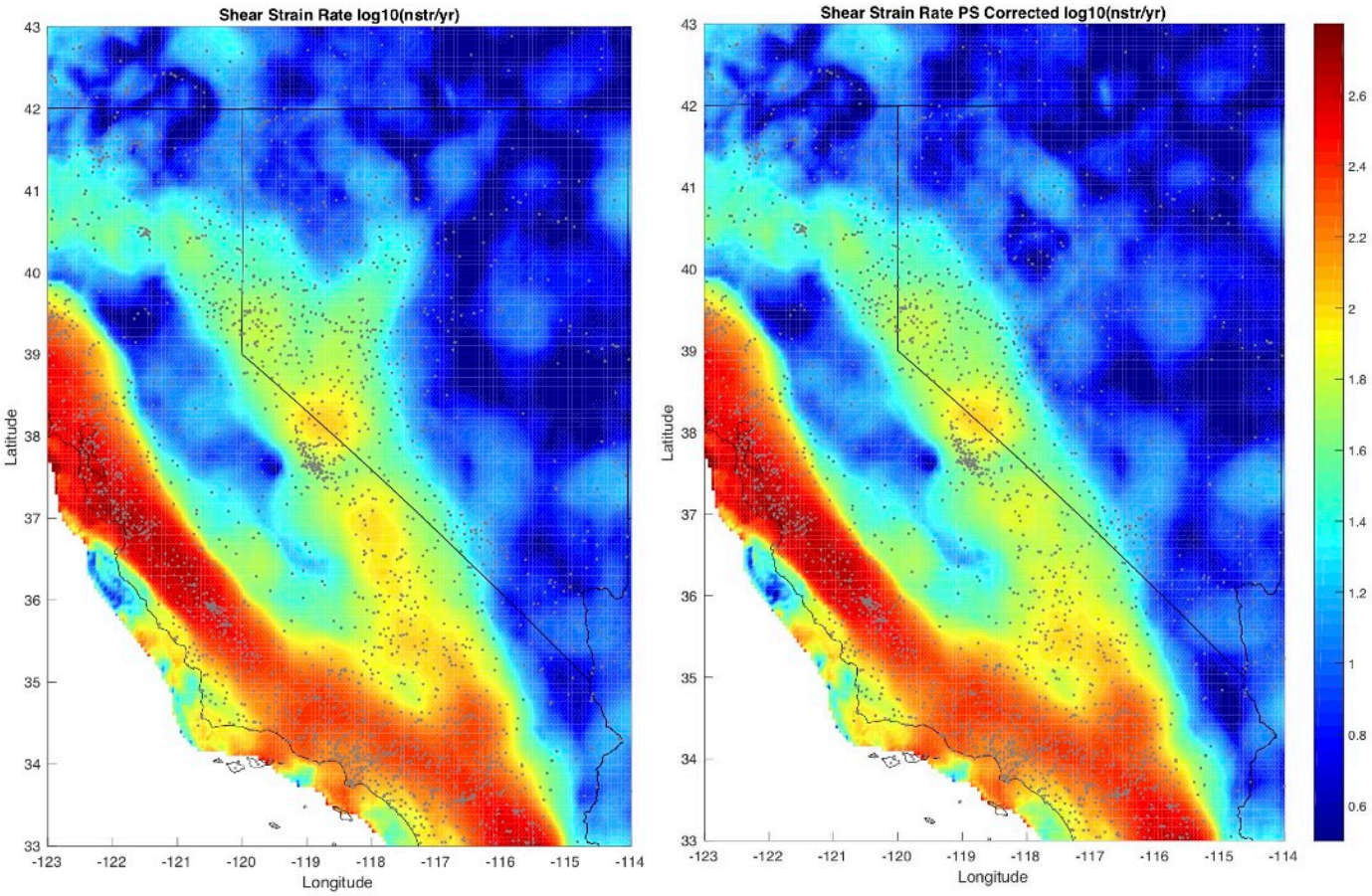

Figure 3b. Same as 3a except for the shear component of the tensor strain rate (left), and for the shear component corrected using a model of viscoelastic relaxation at the CNSB (right).

Correction for CNSB Viscoelastic Relaxation

The maps in Figure 3 show a finger of higher strain rate projecting to the northeast, off the main trend of the WLB, cutting across the velocity contours, in the vicinity of the Central Nevada Seismic Belt (CNSB). In this part of Nevada a sequence of earthquakes from the late 19th to mid-20th century released a large fraction of the historic seismic moment in Nevada and eastern California (*Wallace*, 1984; *Doser, 1988; Savage et al.,* 1995; *Caskey et al*., 2000; *Bell et al*., 2004). This ongoing strain rate anomaly has been attributed to an ongoing viscoelastic relaxation of the upper mantle following the stress change from the earthquakes (*Gourmelen and Amelung*, 2005; *Hetland and Hager*, 2004; *Hammond and Thatcher*, 2004; *Pollitz et al.,* 2008; *Hammond et al.,* 2009; *Dickenson et al.*, 2016). The anomaly appears in the magnitude, shear and dilatation images because it is a uniaxial extension which contains components of both shear and dilatation. It stands out more clearly in the dilatation anomaly because its dilatation rate is larger than the dilatational part of the background WLB tectonic transtension.

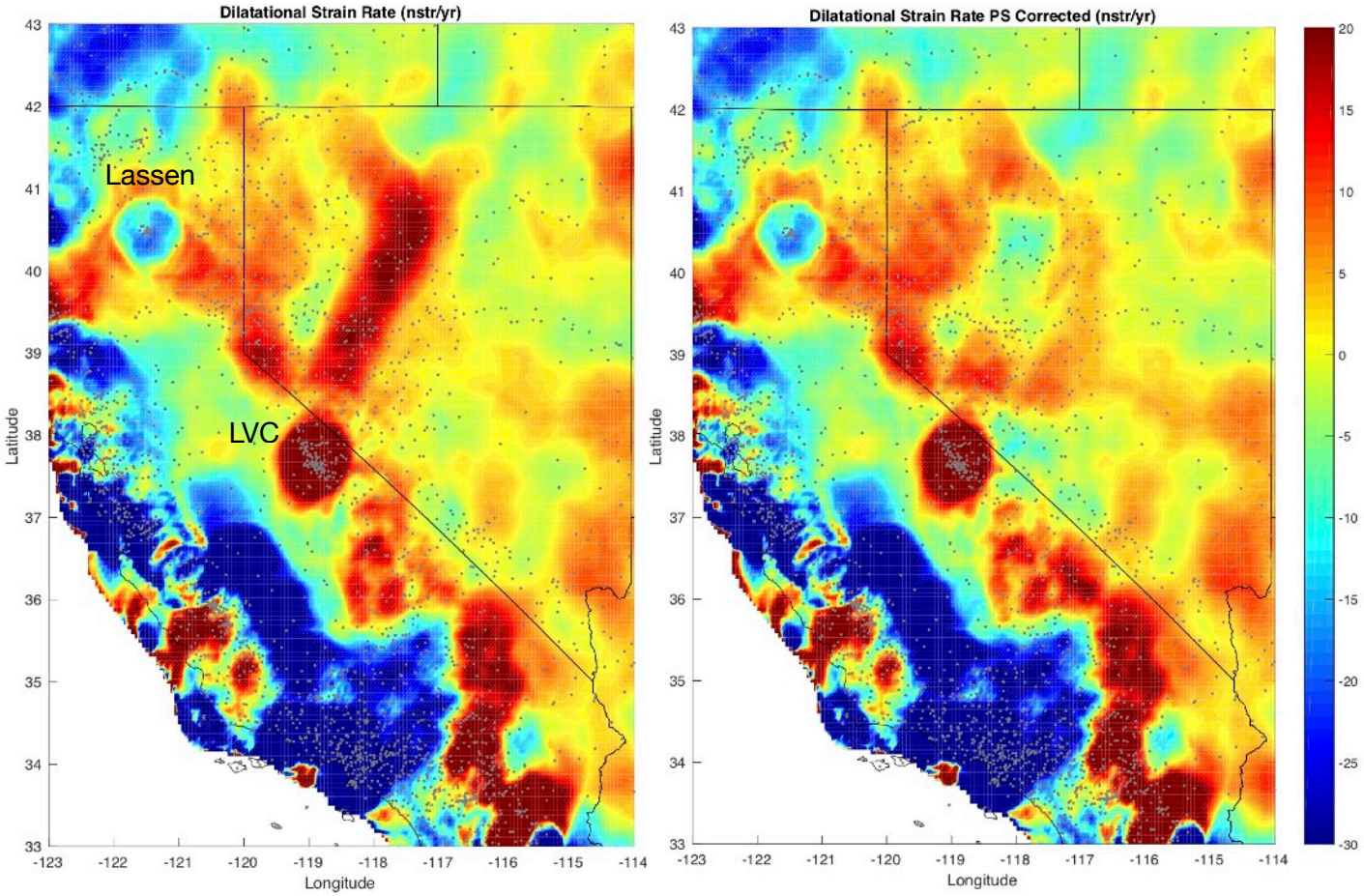

Figure 3c. Same as 3a, except dilatational component of tensor strain rate is shown with a linear color scale (left), and for dilatation component corrected using a model of viscoelastic relaxation at the CNSB (right). Hot colors represent area increase and cool colors represent area decrease. Color scale is in nanostrain/yr.

Because we seek fault slip rates from the geodetic data, we wish to remove decadal scale transients associated with viscoelastic relaxation of the CNSB. To do this we subtract a model of the relaxation processes. Several studies have develop such models, we use the predictions from the suite of models developed by *Hammond et al.,* (2009; 2010) which were developed using the USGS software VISCO1D (*Pollitz*, 1996), and have been used to make functional first order corrections to the strain rate field in several other studies (e.g., *Hammond et al.,* 2011; *Bormann et al.,* 2016). In most places within the WLB the effects on individual slip rates are relatively modest since velocity gradients from decades-to-century old events are smooth and long wavelength (100s of km). We can see from Figure 3b and 3c that the correction removes the CNSB strain rate anomaly. The dilatation shown in Figure 3c is particularly clear, where the extension anomaly has been removed and become even slightly contractional in the near field to the earthquakes, suggesting that the model may slightly over-correct the dilatational strain rates. The over correction is greater near the north end of the Pleasant Valley, 1915 earthquake, whose

source parameters are among the least well known in the model. Thus adjusting the parameters in the model may result in a better model fit. The *Hammond et al.,* (2009), model is based on data now over 12 years old, and may be outdated since the GPS observations in western Nevada have become more numerous and precise over the last decade. Developing better models that satisfy the GPS plus other conditions is an area of active research and will likely continue to improve as more data and innovation are brought to bear on the problem (e.g., *Dickenson et al.*, 2016).

Magmatic Anomalies

The dilatational strain map in Figure 3 shows the presence of transient magmatic strain that is attributable to inflation or deflation from the active volcanoes in eastern California. Two systems stand out clearly in the map. The first is the Long Valley Caldera (LVC) which exhibits a large dilatational anomaly that extends up to 80 km from the center of the magmatic system near the Resurgent Dome (e.g. *Battaglia et al.*, 1999; *Hill*, 2006). Recent analysis of the non-steady component of GPS-measured strain in the Central WLB indicate that the time variable strain rate is correlated with LVC inflation, and also with the timing of hydrological unloading of the Sierra Nevada during the recent drought in California. Seismicity in the Central WLB, including the December 2016 swarm near nine-Mile Ranch in Nevada, between Hawthorne, NV and Lee Vining, CA, may have been triggered by these changes, and reveal an intimate connection between climate, surface loading, magmatic systems and seismic activity (*Hammond et al.,* 2017). This discovery was made because of the attention paid to time variable slip rates near LVC in course of this project. The second magmatic system that is evident in the dilatational strain rate map is Mt. Lassen in northeast, CA. Here the anomaly is contractional, suggesting that Lassen, which erupted over several years starting in 1914, (*Clynne et al.,* 1999), may now be in a different period of its volcanic cycle, experiencing either thermal contraction or draining of its magma system. The radii of the circular anomalies are partly a function of the width of the Gaussian weighting kernel used in the imaging, but provides a conservative zone inside which geodetic data should be excluded in order to remove magmatic transients from the data.

Block Modeling

Spontaneous Blocks Model Construction

In this analysis I introduce a new modeling technique where the blocks generate themselves given an input fault database and rectangular box denoting intervals of latitude and longitude that bounds an area inside which slip rates will be modeled. Automating this step in model construction reduces the potential for analyst bias in model generation. For example, connecting fault segments that close to one another, but are not connected in the database with block boundaries is tempting in by-hand model construction because the human sees how deformation could be through-going, though this interpretation may only be one of several that are permissible by the data, and not necessarily representative of true fault interaction or rupture in the next earthquake. Automation also reduces the amount of time required to generate models

and so allows more time to be dedicated to testing other features of the modeling, including various regularization strategies, fault databases, combinations with geologic data, etc.

The Algorithm

Here I provide a sketch of the algorithm used to generate each block model.

1) Read in fault database, currently the set of sources from the 2014 version of the USGS seismic hazard map is chosen.
2) Specify a latitude longitude box, usually large enough to contain several full fault systems, but within the area covered by the fault database, and small enough to keep run time small.
3) Generate block model
    a) Truncate, trim, simplify the set of faults to those within the box
    b) Perform a Delaunay triangulation of nodes defining the box boundary and simplified fault traces.
    c) Create a legal block model where each triangle is a block and incorporates the geologic data on fault traces, locking depths and dips.
    d) Begin a loop where the model is iteratively simplified, reducing the number of blocks by:
        i) Scoring segments according to their connectively to the faults
        ii) Removing low scoring segments by combining blocks bounded by low scoring segments (subject to model condition checks)
        iii) Remove blocks that have very low aspect ratios (subject to checks)
        iv) Remove blocks that are very small (subject to checks)
        v) Remove blocks that have very small interior angles (subject to checks)
        vi) Remove blocks that are have irregular shapes (subject to checks)
        vii) Perform important checks on model viability
        viii) If the number of blocks is smaller than a predetermined threshold or has not changed since the last iteration, end loop, otherwise repeat.
4) Remove all blocks that are not covered by the gridded velocity field
5) Compute model regularization parameters
6) Solve for slip rates using model and gridded velocity field

The code is written in the Matlab programming language, with minimal toolboxes. An example of the process for one model of the Southern Walker Lane is shown in Figure 4. This model represents one of a large number of models that are generated.

Solution for Slip Rates

We solve for block rotations and slip rates in a simultaneous regularized least squares inversion using the method described in *Hammond and Thatcher*, 2007 and *Hammond et al.*, 2011. The the regularization parameters for each fault are adjusted using, as a starting point, constant values derived in those studies. However, we further customize the damping of slip rates by using the

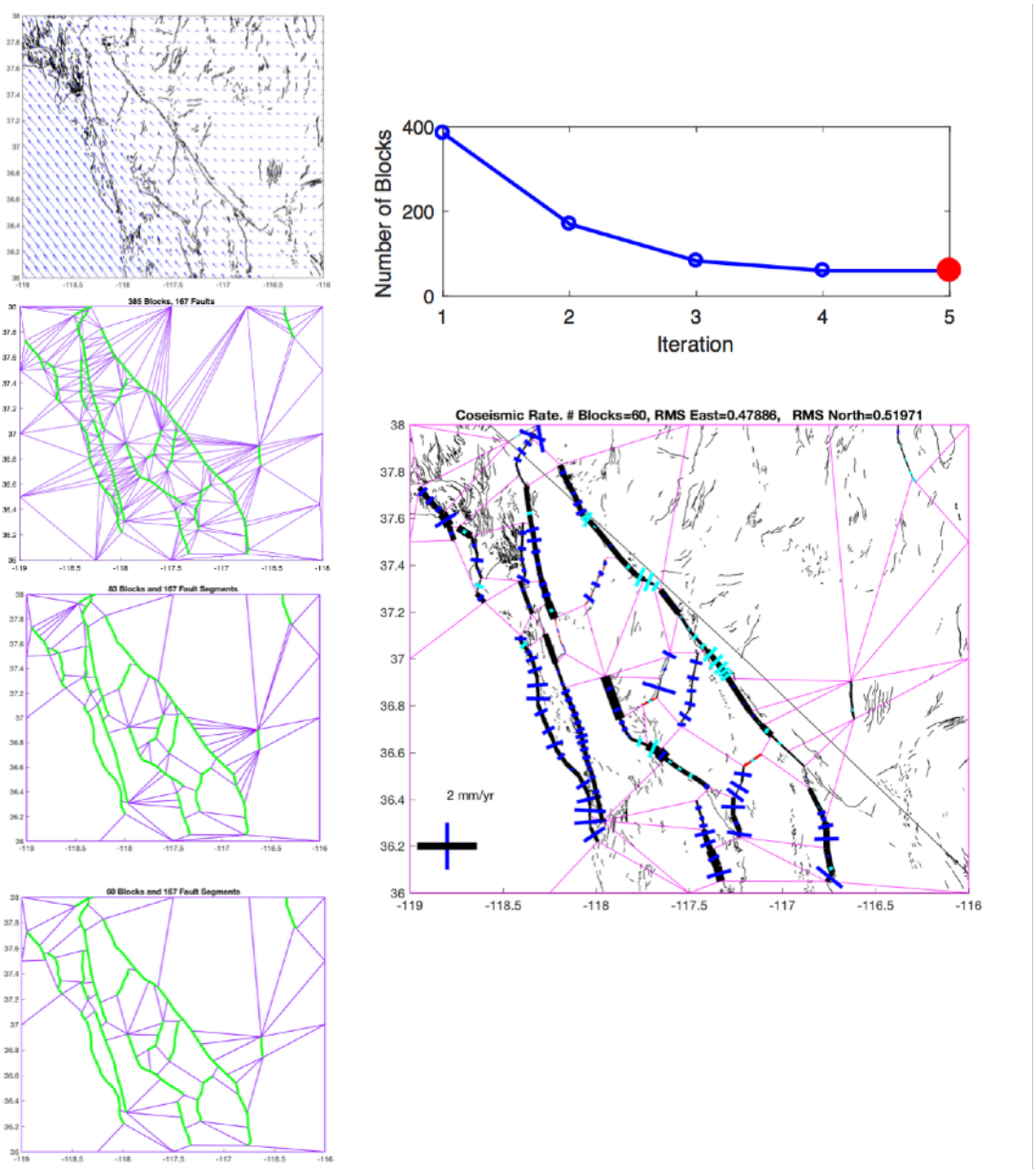

Figure 4. Example of Spontaneous Block model generation. Top left panel shows gridded velocity field and faults from the USGS Quaternary Fault and Fold Database. Second panel down shows the sources used in the 2014 edition of the USGS seismic hazard map (green line segments), and triangular blocks automatically built around them. Subsequent panels downward show how the number of blocks is iteratively reduced by the algorithm, with number of blocks remaining after each iteration shown in the upper right. The bottom right panel shows the slip rate estimates made from the final model.

strain rate model shown in Figure 3. We extract for each fault a representative value for the magnitude of the strain rate field by sampling the strain rate at the mid-point of the fault. We then relate the strain rate to a slip rate using a function that is derived from the relationship

between the strain rate model with postseismic relaxation correction applied and the maximum geologic slip rate present in the USGS sources database from the 2014 hazard map (*Petersen et al.,* 2014) and the UCERF3 database (*Field et al.,* 2013). This relationship is shown in Figure 5. This step allows for balanced model solutions in very different tectonic environments (e.g., San Andreas Fault system versus eastern Nevada Basin and Range), where the fault slip rates and GPS velocity signal to noise ratio may differ by orders of magnitude from one place to the other. Once this regularization slip rate (RSR) is estimated, it is applied as a damping parameter to the inversion for slip rate, where the condition is that the slip rates is equal to zero subject to the prior uncertainty of the RSR.

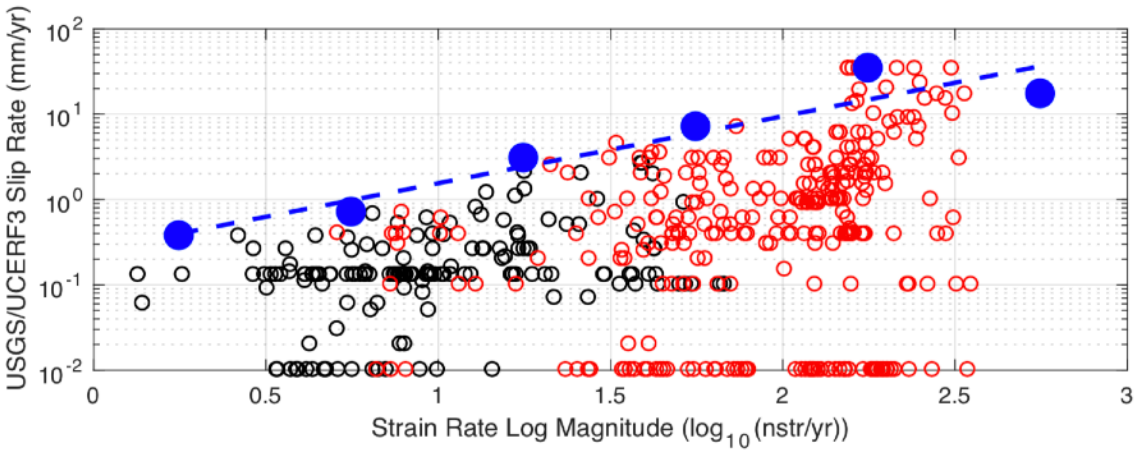

Figure 5. Plot of fault slip rate from the USGS source fault database (*Petersen et al.,* 2014) (black) and the UCERF3 database (*Field et al.,* 2013) (red) versus the associated strain rate values as extracted from Figure 3b. The blue dots are the maximum values inside bins of width one half of a $\log_{10}$ strain rate magnitude in nanostrain/yr. The blue dashed line represents the best fitting line to these data and is used to relate strain rate to the RSR value.

Grid of models

Having a tool that automatically generates block models from a given fault database is advantageous because it is now possible to generate not just a single mode, but many, eventually thousands of models with many estimates for each fault based on different realizations of the block generation algorithm. Each realization is based on a the same fault database but on a model domain generated from a slightly different input grid boundary domain. This allows for generating posterior distributions of slip rate that account for uncertainties associated with velocity data and block geometry. This methodology is now functional and long runs generating WLB slip rates for the faults in the USGS database of sources (*Petersen et al.,* 2014) are now in progress.

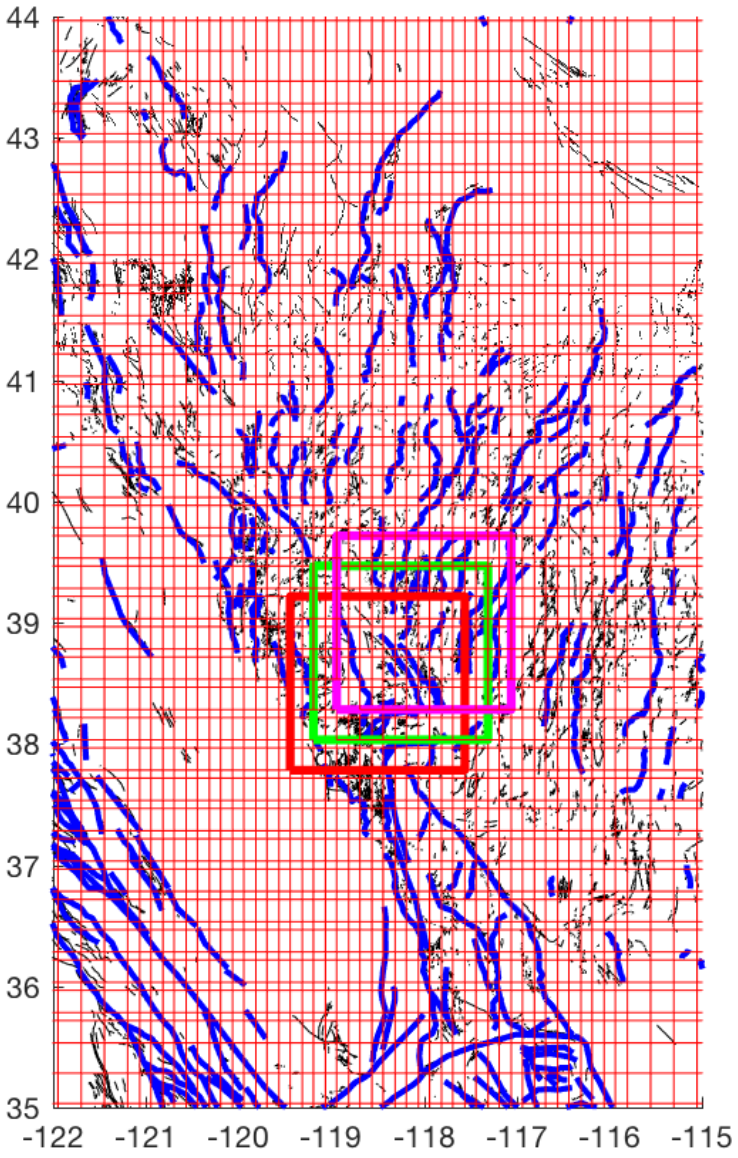

Figure 6. Example grid domain showing overlapping boundaries of many block models. Example model domains shown in red, green and magenta boundaries in this case are 1.9˚x1.4˚ in longitude/ latitude size, each containing model faults for the Wassuk and Benton Springs faults.

Conclusions

GPS Imaging is a new method for robust estimation of velocity and strain rate fields from GPS data. This project has brought GPS Imaging into the realm of fault slip rate estimation. While the technique was developed originally for stabilizing and easing interpretation of the of signals

of vertical motion in GPS velocity fields, it is now applied to horizontal motions in California and Nevada to image the WLB strain rate field and estimate faults slip rates.

The strain rate model presented in Figure 3 clearly shows the well-known active tectonic transtension in the WLB, east of the Sierra Nevada/Great Valley microplate. This strain is fastest in the southern Walker Lane, across Owens Valley near the Sierra Nevada. The images show the anomalies associated with transient magmatic inflation at LVC and contraction near Lassen Peak. They also show a positive dilatation anomaly at the Central Nevada Seismic Belt, which is thought to be a transient earthquake cycle-related deformation from viscoelastic relaxation of the upper mantle. We tested a model of this process (*Hammond et al.*, 2009) which adequately corrected for this anomaly, but the latest data reveal that the fit is not perfect, suggesting that the model could be improved. In the future we will compare more recently constructed models (e.g. *Dickenson et al.,* 2016) and/or develop a new model that fits data more closely.

GPS imaging clearly reveals transient strain from magmatic anomalies at the Long Valley Caldera and at Mt. Lassen in northeast, CA. Recent analysis of the non-steady component of GPS-measured strain in the Central WLB indicate that the time variable strain rate is correlated with LVC inflation, and also with the timing of hydrological unloading of the Sierra Nevada during the recent drought in California. Seismicity in the Central WLB, including the December 2016 swarm near nine-Mile Ranch in Nevada, between Hawthorne, NV and Lee Vining, CA, may have been triggered by these changes, and reveal an intimate connection between climate, surface loading, magmatic systems and seismic activity (*Hammond et al.,* 2017). This discovery was made because of the attention paid to time variable slip rates near LVC in course of this project. Investigation of these effects is continuing.

I have developed and new analysis method for estimating slip rates on faults in zones where the deformation is spatially variable, fault networks are complex. Spontaneous Block models build themselves from the original data on fault trace geometry, dips, locking, sense of slip. Many models are generated to estimate a distribution of slip rates for each fault in order to understand the component of slip rate uncertainty that is attributable to choices in model construction. The model regularization includes a customization that scales the apriori slip rate damping in the inversion with the strain rate magnitude, making the method applicable in California and Nevada where strain rates vary by orders of magnitude.

Bibliography of publications resulting from this award to date

Published Abstracts

Hammond, W.C., C. Kreemer, G. Blewitt, 2018, Robust estimation of fault slip rates using GPS Imaging in the Walker Lane and Western Great Basin, 2018 Working Group on Nevada Seismic Hazards, February 5-7, Reno, Nevada.

Bormann, J., W.C. Hammond, C. Kreemer, G. Blewitt, 2018, GPS constraints on present-day slip rates in the northernmost Walker Lane: Reno, Carson City, and Tahoe region, Nevada and California, 2018 Working Group on Nevada Seismic Hazards, February 5-7, Reno, Nevada.

Hammond, W.C., G. Blewitt, 2016, GPS Imaging of time-variable earthquake hazard: The Hilton Creek fault, Long Valley California, Abstract G51B-1112, Fall AGU Meeting, San Francisco, CA.

Hammond, W.C., C. Kreemer, G. Blewitt, 2017, GPS Imaging suggests links between climate, magmatism, seismicity, and tectonics in the Sierra Nevada-Long Valley Caldera-Walker Lane system, western United States, Abstract G41A-02, Fall AGU Meeting, New Orleans, LA, Dec. 11-15, 2017.

Hammond, W.C., 2017, Effects of water on active crustal deformation in California and Nevada from GPS data, NSF EarthScope Hydrogeodesy Synthesis Workshop, UC San Diego, Scripps IGPP, October 25-27, 2017, [INVITED].

Hammond, W.C., and L. Flesch, 2017, Eye-popping EarthScope Science: A synthesis, celebration and exploration of new horizons for geodetic and geodynamic imaging, Plenary Talk at EarthScope National Meeting, Anchorage Alaska, May 26-28, 2017 [INVITED].

Workshop report

Anderson. J., R. Kohler, et al., (+18 coauthors), 2018, Report by the 2018 Nevada Working Group, 2018 Working Group on Nevada Seismic Hazards, meeting February 5 and 6, Reno, Nevada.

Manuscript in preparation

Hammond, W.C., C. Kreemer, G. Blewitt, 2018, Robust estimation of fault slip rates in the Walker Lane from GPS data using spontaneous blocks, in prep.

References

Amos, C.B., K. I. Kelson, D. H. Rood, D. T. Simpson, R.S Rose, 2015, Late Quaternary slip rate on the Kern Canyon fault at Soda Spring, Tulare County, California, *Lithosphere*, *v. 2*; n. 6; p. 411–417, doi: 10.1130/L100.1.

Anderson, J., G. Biasi, 2016, What is the basic assumption for probabilistic seismic hazard assessment? *Seismological Research Letters, v 87*, n. 2A, p 323-326, doi: 10.1785/0220150232.

Battaglia, M., C. Roberts, P. Segall, 1999, Magma intrusion beneath Long Valley Caldera confirmed by temporal changes in gravity *Science 285*, 2119 DOI: 10.1126/science. 285.5436.2119

Bell, J.W., S.J. Caskey, A.R. Ramelli, L. Guerrieri, 2004, Pattern and rates of faulting in the Central Nevada Seismic Belt, and paleoseismic evidence for prior beltlike behavior, *Bull. Seis. Soc. America, Vol. 94*, No. 4, pp. 1229–1254.

Bennett, R.A., W. Rodi, R.E. Reilinger, 1999, Global Positioning System constraints on fault slip rates in southern California and northern Baja, Mexico, *J. Geophys. Res.*, v 101, B10, p. 21,943-21,960.

Bird, P. and C. Kreemer, 2015, Revised tectonic forecast of global shallow seismicity based on version 2.1 of the Global Strain Rate Map, *Bull. Seis. Soc. America, v. 105*, no. 1 pp. 152-166, doi:10.1785/0120140129.

Blewitt, G., C. Kreemer, W.C. Hammond. J. Goldfarb, 2013, Terrestrial reference frame NA12 for crustal deformation studies in North America, *J. Geodynamics*, 72, pp. 11-24, ISSN 0264-3707, http://dx.doi.org/10.1016/j.jog.2013.08.004.

Blewitt, G., C. Kreemer, W.C. Hammond, J. Gazeaux, 2016, MIDAS trend estimator for accurate GPS station velocities without step detection, 121, *J. Geophys. Res*., doi: 10.1002/2015JB012552.

Bormann, J., W.C. Hammond, G. Blewitt, C. Kreemer, S. Jha, 2013, A synoptic model of fault slip rates in the Eastern California Shear Zone and Walker Lane from GPS velocities for seismic hazard studies, SSA Annual Meeting, Salt Lake City, Utah, April 17-19, 2013.

Bormann, J., W.C. Hammond, C. Kreemer, G. Blewitt, 2016, Accommodation of missing shear strain in the Central Walker Lane, western North America: Constraints from dense GPS measurements, *Earth Planet. Sci. Lett.*, doi: 10.1016/j.epsl.2016.01.015.

Briggs, R.W. and S. G. Wesnousky, 2004, Late Pleistocene fault slip rate, earthquake recurrence, and recency of slip along the Pyramid Lake fault zone, northern Walker Lane, United States, *J. Geophys. Res., 109,* B08402, doi:10.1029/2003JB002717.

Caskey, S. J., J. W. Bell, D. B. Slemmons, and A. R. Ramelli, 2000, Historical surface faulting and paleoseismology of the central Nevada seismic belt, in *Great Basin and Sierra Nevada*, D. R. Lageson, S. G. Peters, and M. M. Lahren (Editors), Geological Society of America, Boulder, Colorado, Geological Society of America Field Guide 2, 23–44.

Caskey, S.J., J.W. Bell, A.R. Ramelli, S.G.Wesnousky, 2004, Historic surface faulting and paleoseismicity in the area of the 1954 Rainbow Mountain–Stillwater Earthquake Sequence, Central Nevada, *Bull. Seis. Soc. America, v. 94*, No. 4, pp. 1255–1275.

Clynne, M. A., R. L. Christiansen, T. J. Felger, P. H. Stauffer, and J. W. Hendley, 999, Eruptions of Lassen Peak, California, 1914 to 1917, U.S. Geol. Surv. Fact Sheet, 172–98, 2.

Dickinson, H., A. M. Freed, and C. Andronicos, 2016, Inference of the viscosity structure and mantle conditions beneath the Central Nevada Seismic Belt from combined postseismic and lake unloading studies, *Geochem. Geophys. Geosyst., 17*, doi:10.1002/2015GC006207.

Doser, D., 1988, Source parameters in earthquakes in the Nevada seismic zone, 1915-1943, *J. Geophys. Res. v* 93**,** B12**,** 15,001–15,015.

Faulds, J.E., and Henry, C.D., 2008, Tectonic influences on the spatial and temporal evolution of the Walker Lane: An incipient transform fault along the evolving Pacific – North American plate boundary, *in* Spencer, J.E., and Titley, S.R., eds., Ores and orogenesis: Circum-Pacific tectonics, geologic evolution, and ore deposits: Arizona Geological Society Digest 22, p. 437-470.

Field, N., et al., 2013, Uniform California earthquake rupture forecast, Version 3 (UCERF3) - The time-independent model, USGS Open-File Report 2013-1165, CGS Special Report 228, SCEC publication 1792.

Gourmelen, N., and F. Amelung, 2005, Postseismic relaxation in the Central Nevada Seismic Belt, *Science v. 310*, p 1473-1476.

Haddon, E.K., C.B. Amos, O. Zielke, A.S. Jayko, R. Bürgmann, 2016, Surface slip during large Owens Valley earthquakes, *Geochemistry, Geophysics, Geosystems*, doi: 10.1002/2015GC006033.

Hammond, W. C., and W. Thatcher, 2007, Crustal deformation across the Sierra Nevada, northern Walker Lane, Basin and Range transition, western United States measured with GPS, 2000–2004, *J. Geophys. Res., 112*, B05411, doi:10.1029/2006JB004625.

Hammond, W.C., C. Kreemer, G. Blewitt, 2009, Geodetic constraints on contemporary deformation in the northern Walker Lane: 3, Central Nevada seismic belt postseismic relaxation, *in* Oldow J.S. and Cashman, P.H. H., eds., *Late Cenozoic Structure and Evolution of the Great Basin–Sierra Nevada Transition*: Geological Society of America Special, Paper 447, p. 1–15, doi:10.1130/2009.2447(01).

Hammond, W.C., Kreemer, C., Blewitt, G., Plag H.-P., 2010, The effect of viscoelastic postseismic relaxation on estimates of interseismic crustal strain accumulation at Yucca Mountain, Nevada, *Geophys. Res. Lett.*, 37, L06307, doi:10.1029/2010GL042795.

Hammond, W. C., G. Blewitt, and C. Kreemer, 2011, Block modeling of crustal deformation of the northern Walker Lane and Basin and Range from GPS velocities, *J. Geophys. Res.,* 116, B04402, doi:10.1029/2010JB007817.

Hammond, W.C., G. Blewitt, C. Kreemer, 2016, GPS Imaging of vertical land motion in California and Nevada: Implications for uplift of the Sierra Nevada, *J. Geophys. Res.*, doi: 10.1002/2016JB013458.

Hammond, W.C., C. Kreemer, G. Blewitt, 2017, GPS Imaging suggests links between climate, magmatism, seismicity, and tectonics in the Sierra Nevada-Long Valley Caldera-Walker Lane system, western United States, Abstract G41A-02, Fall AGU Meeting, New Orleans, LA, Dec. 11-15, 2017.

Hearn, E. H., and E.D. Humphreys, 1998, Kinematics of southern Walker Lane Belt and motion of the Sierra Nevada block, California, *J. Geophys, Res.*, v. 103, B11, p 27,033-27,049.

Hetland, E. A., and B. H. Hager, Postseismic relaxation across the Central Nevada Seismic Belt, *J. Geophys. Res., v. 108* B8, 2394, doi:10.1029/2002JB002257, 2003.

Hill, D.P., 2006, Unrest in Long Valley Caldera, California, 1978-2004, in C. Troise, G. De Natale, C.R.J. Kilburn, Mechanisms of Activity and Unrest at Large Calderas, Geological Society of London Special Publication 269, p 1-24.

Koehler, R. D. and S. G. Wesnousky, 2011, Late Pleistocene regional extension rate derived from earthquake geology of late Quaternary faults across the Great Basin, Nevada, between 38.5°N and 40°N latitude, *GSA Bulletin v. 123,* no. 3/4; p. 631–650, doi: 10.1130/B30111.1.

Kreemer, C., W.C. Hammond, G. Blewitt, A. Holland, R.A. Bennett, 2012, A geodetic strain rate model for the southwestern United States, scale 1:1,500,000, Nevada Bureau of Mines and Geology publication M178.

Kreemer, C., G. Blewitt, and E. C. Klein, 2014, A geodetic plate motion and Global Strain Rate Model, *Geochem. Geophys. Geosys*., 15, 3849–3889, doi:10.1002/2014GC005407.

Lee, J., J. Spencer, L. Owen, 2001, Holocene slip rates along the Owens Valley fault, California: Implications for the recent evolution of the Eastern California Shear zone, *Geology,* v. 29; no. 9, p. 819–822.

McCaffrey, R., 2005, Block kinematics of the Pacific–North America plate boundary in the southwestern United States from inversion of GPS, seismological, and geologic data, *J. Geophys. Res.,* 110, B07401, doi:10.1029/2004JB003307.

Meade, B. J., and B. H. Hager, 2005, Block models of crustal motion in southern California constrained by GPS measurements, *J. Geophys. Res.,* 110, B03403, doi: 10.1029/2004JB003209.

Oldow, J., C.L.V. Aiken, J.L. Hare, J.F. Ferguson, R.F. Hardyman, 2001, Active displacement transfer and differential block motion in the Central Walker Lane, western Great Basin, *Geology*, v. 29, no 1. p 19-22.

Oldow, J., 2003, Active transtensional boundary zone between the western Great Basin and Sierra Nevada block, western U.S. Cordillera, *Geology*, v. 29, no 1. p 19-22.

Pancha, A., Anderson, J.G., and Kreemer, C., 2006, Comparison of seismic and geodetic scalar moment rates across the Basin and Range province, *Bull. Seis. Soc. America*, *v. 96*, p. 11-32.

Petersen, M. D., M. P. Moschetti, P. M. Powers, C. S. Mueller, K. M. Haller, A. D. Frankel, Y. Zeng, S. Rezaeian, S. C. Harmsen, et al., 2014a, Documentation for the 2014 update of the United States national seismic hazard maps, U.S. Geol. Surv. Open-File Rept. 2014- 1091, 243 pp., doi: 10.3133/ofr20141091.

Petersen, M.D., Y. Zeng, K.M. Haller, R. McCaffrey, W.C. Hammond, P. Bird, M Moschetti, Z. Shen, J. Bormann, and W. Thatcher, 2014b, Geodesy- and geology-based slip-rate models for the Western United States (excluding California) national seismic hazard maps: U.S. Geological Survey Open-File Report 2013–1293, 80 p., http://dx.doi.org/10.3133/ofr20131293.

Pollitz, F., 1996, Coseismic deformation from earthquake faulting on a layered spherical earth, *Geophys. J. Int.*, 125, 1-14.

Pollitz, F. F., P. McCrory, J. Svarc, and J. Murray, 2008, Dislocation models of interseismic deformation in the western United States, *J. Geophys. Res., 113*, B04413, doi: 10.1029/2007JB005174.

Ramelli, A.R., J.W. Bell, C.M. dePolo, J.C. Yount, 1999, Large-magnitude, Late Holocene earthquakes on the Genoa Fault, west-central Nevada and eastern California, *Bull. Seis. Soc. America,v.* 89, 6, pp. 1458-1472.

Savage, J., and R. Burford, 1973, Geodetic determination of relative plate motion in central California, *J. Geophys. Res., 78*, 832–845.

Savage, J., M. Lisowski, J.L. Svarc, W.K. Gross, 1995, Strain accumulation across the central Nevada seismic zone, 1973-1994, *J. Geophys. Res, v. 100*, n. B10, p 20.257-20,269.

Savage, J., W. Gan, J.L. Svarc, 2001, Strain accumulation and rotation in the Eastern California Shear Zone, *J. Geophys. Res., v106,* B10, p 21,995-22,007.

Shen, Z.-K., D.D. Jackson, B.X. Ge, 1996, Crustal deformation across and beyond the Los Angeles basin from geodetic measurements, *J. Geophys. Res., v. 101,* B12, p. 27,957-27,980.

Stewart, J.H., 1988, Tectonics of the Walker Lane belt, western Great Basin: Mesozoic and Cenozoic deformation in a shear zone, *in* Ernst, W.G., ed., Metamorphism and crustal evolution of the western United States: Englewood Cliffs, New Jersey, Prentice-Hall, p. 681–713.

Wallace, R. E., 1984, Patterns and timing of Late Quaternary faulting in the Great Basin province and relation to some regional tectonic features, *J. Geophys. Res., v.* 89**,** 5763–5769.

Ward, S. N., 1998, On the consistency of earthquake moment rates, geological fault data, and space geodetic strain: the United States, *Geophys. J. Int., v.134*, 172-186.

Wesnousky, 2005, Active faulting in the Walker Lane, *Tectonics*, v. 24, TC2009, doi: 10.1029/2004TC001645.

Wesnousky, S., J. Bormann, C. Kreemer, W.C. Hammond, J. Brune, 2012, Neotectonics, geodesy and seismic hazard in the northern Walker Lane of western North America: Thirty kilometers of crustal shear and no strike-slip? *Earth and Planetary Science Letters,* v. 329-330, 133–140, doi:10.1016/j.epsl.2012.02.018.

Williams, S. P. D., 2003, The effect of coloured noise on the uncertainties of rates estimated from geodetic time series, *Journal of Geodesy*, 76: 483–494 DOI 10.1007/ s00190-002-0283-4.